SURFACE MORPHOLOGY OF RANDOM POROUS MATERIALS STUDIED BY IMAGE ANALYSIS OF SERIAL FOCUSSING PLANES

Helmut Hermann, Roland Hübel and *Cullie J. Sparks

Institute of Solid State Research and Materials Science, Helmholtzstr.20,
PF 16, D-O-8027 Dresden, Germany
*Metals and Ceramics Divison, Oak Ridge National Laboratory, P.O.Box 2008,
Oak Ridge, TN 37831, USA

ABSTRACT

The surface morphology of a random powder typical of that used in powder diffraction is analyzed in terms of lateral second-order correlations and their variation with distance of a reference plane parallel to the surface. The experimental data are obtained from optical micrographs of subsequent focussing planes using suitable image analysis routines. The procedure turns out to be a non-destructive method for serial planar section analyses of rough surfaces.

Keywords: image analysis, porosity, random materials, second-order characteristics, serial sectioning, surface morphology.

INTRODUCTION

The surface morphology of solids may affect many physical and chemical properties such as optical properties (Brodsky and Urbakh, 1990), catalytic reactions (Seri-Levi, 1991) absorption of X-rays (Hermann and Ermrich, 1987, Sparks et al., 1991) etc. Some work has been done to define characteristic parameters of surface morphology and to propose experimental methods for their measurement. Coster (1992) reviewed morphological tools for the analysis of rough surfaces based on classical stereological parameters. The surface is described by its local height with respect to a reference plane, the volume below the surface, the surface area and the connectivity number which define the essential (first-order) parameters. Similar quantities can be defined for vertical sections of surfaces. More detailed description of rough surfaces requires the definition and experimental measurement of second-order parameters (Vedel-Jensen and Kiêu, 1992). An example is the height-height correlation function used by Savage et al. (1991).

In the present paper we propose a method for the characterization of random surfaces which is based on the observation (Jähne, 1991) and digital analysis of serial, equidistant, parallel focussing planes. For non-overlapping surfaces, the method corresponds to a complete three-dimensional analysis by means of serial sectioning. The surface morphology parameters accessible by the present method are discussed in terms of a variable structure model for surface and bulk structure of random porous materials. The method is applied to characterize the surface of a powder sample.

STRUCTURE MODEL

The bulk structure of random porous substances such as powders and sintered materials can be simulated by means of the well-known Boolean model (for review see Serra, 1982, Stoyan et al., 1987, and references therein). The model is based on the generation of a random (Poisson) field of points (germs) and a sequence of geometrical objects (grains). Each germ is covered by one of the grains. The union of all grains forms a random set A. We use the set A to describe the distribution of the solid material whereas the complement $B = A^c$ of A represents the pores. The surface is simulated by a planar section of the infinitely extended bulk structure. If the planar section is smooth the surface of the porous model is called smooth as well. If the planar section of the model is fuzzy at dimensions comparable to the size of its pores and grains, the surface is called rough (or non-planar). The term "roughness" is used here in the phenomenological sense but not as "surface area per reference surface area" (Coster, 1992). Figure 1 illustrates the model.
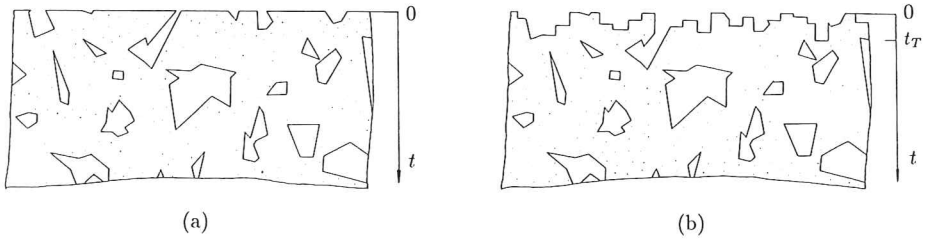

(a)   (b)

Figure 1: Smooth (a) and rough (b) surface of a porous material. The bulk structure is simulated by a Boolean model. Here, the primary grains are random Poisson polyhedra. The surface results from a step-like (a) and a continuous (b) decrease of the volume fraction from the bulk value realized for $t \geq t_T$ to zero at $t = 0$. Parameter t_T characterizes the profile fluctuation due to surface roughness ($t_T = 0$ in (a) and $t_T > 0$ in (b), $t = 0$ is the surface reference plane).

Now we compile those quantitative relationships which will be necessary for the discussion and determination of model parameters from experimental data. (For a rigorous mathematical treatment see Stoyan et al., 1987).

Single grains (and particles) are characterized by the mean volume, $\bar{V}$, mean surface area, $\bar{S}$, mean chord length $\bar{l} = 4\bar{V}/\bar{S}$, and mean distance probability function

$$\bar{\gamma}(r) = \frac{1}{4\pi} \langle \int_\Omega \int_V s_i(\vec{u}) s_i(\vec{u} + \vec{r}) dV_u \, d\Omega \rangle_i, \quad s_i(\vec{r}) = \begin{cases} 1, & \vec{r} \in i\text{-th grain} \\ 0, & \text{otherwise.} \end{cases} \quad (1)$$

The brackets $\langle \cdots \rangle_i$ denote the average over all particles, i, dV_u is the volume element situated at the endpoint of vector $\vec{u}$, and $d\Omega$ is the increment of the solid angle. Characterizing the grains of the Boolean model by $\bar{V}, \bar{S}$ and $\bar{\gamma}(r)$, the following expressions hold:

$$c_A = 1 - \exp(-\lambda \bar{V}), \quad (2)$$

$$\bar{l}_B = \frac{4}{\lambda \bar{S}} = \frac{4\bar{V}}{\bar{S}} \frac{1}{\ln(1 - c_A)^{-1}}, \quad (3)$$

$$\bar{l}_A = \frac{c_A}{1 - c_A} \bar{l}_B, \quad (4)$$

$$f(x_B) = \frac{1}{\bar{l}_B} \exp(-x_B/\bar{l}_B), \quad (5)$$

where λ is the density of the germs, c_A the volume fraction of the random set A, $\bar{l}_A$ and $\bar{l}_B$ is the mean chord length of A and $B = A^c$, respectively, and $f(x_B)$ is the probability density of the distance between an arbitrary point in B and the boundary of B in an arbitrary direction (density of the linear contact distribution function).

The covariance

$$C_A(r) = 2c_A - 1 + (1 - c_A)^2 \exp[\lambda\bar{\gamma}(r)], \qquad (6)$$

is defined by the probability of finding two random points in A having distance r. It represents second-order properties of the model. The following (and further) first-order characteristics can be calculated from $C_A(r)$:

$$c_A = C_A(0), \qquad (7)$$

$$S_V = -4 \lim_{r \to 0} \frac{dC_A(r)}{dr}, \qquad (8)$$

$$\bar{l}_B = 4\frac{1 - c_A}{S_V} \qquad (9)$$

(see Stoyan et al., 1987, pp. 176, 177, 180) where S_V is the mean surface area per unit volume. We use the Boolean model to simulate the bulk properties of the material specifying $\lambda = \lambda_b = const.$ for $t \geq t_T$ (homogeneous Boolean model). The surface roughness is simulated by thinning the bulk material in the vicinity ($0 \leq t \leq t_T$) of the surface. This corresponds to an inhomogeneous Boolean model where both $\bar{V} = \bar{V}(t)$ and $\lambda = \lambda(t)$ may vary in the depth region $0 \leq t \leq t_T$. At $t \geq t_T$ we have $\lambda = \lambda_b$, $\bar{V} = \bar{V}_b$ where $\bar{V}_b$ is the mean volume of a grain of the Boolean model simulating the bulk structure.

In the following section we explain a procedure for a more detailed investigation of the surface morphology of porous materials.

OBSERVATION METHOD AND IMAGE ANALYSIS

Micrographs for a series of subsequent focussing planes are recorded utilizing an optical microscope. The positions $t_k = k\Delta t, k = 1, \ldots, n$, of the focussing planes with respect to the axis t perpendicular to the surface reference plane are calibrated by means of an suitable linear grid situated in the focussing range with a small angle between reference plane, $t = 0$, and grid. The depth resolution, Δt, of the microscope is estimated in the same way.

Figure 2a shows an example of an optical micrograph of a powder sample. The micrograph is transformed into a grey value image by means of a CCD camera then stored and analyzed with a Quantimet 570 image processing system. The analysis is done according to the following procedure: Those regions of the sample situated in the depth interval $(t_k - \Delta t, t_k)$ are characterized by sharp and very local grey value fluctuations. They are selected by a morphological top-hat transformation. It starts with an opening. The corresponding erosion (5 cycles, octagon structuring element) removes all small bright regions, whereas, subsequent dilation (also 5 cycles, same structuring element) restores the original size of the regions remaining after erosion. The resulting smoothed grey value image (see figure 2b) is subsequently substracted from the original image. The difference comprises the grey value fluctuations caused by the fine structure of the well-focussed regions of the sample. Choosing a suitable grey level, one obtains a binary image (figure 2c) characterizing the distribution of sample regions situated in the depth interval $(t_k - \Delta t, t_k)$. The most suitable grey level value is interactively estimated by comparison

of the original and the binary image. The binary image consists of a large number of small disconnected image sectors representing the positions of sharp grey value fluctuations of the original micrograph. It is reasonable to assume that the region between neighbouring image sectors is also situated in the depth interval $(t_k - \Delta t, t_k)$ if the distance between these regions is of the order of magnitude Δt. Therefore, the top-hat and binary transformations are followed by a binary closing procedure (consecutive dilation and erosion, 10 cycles, octagon structuring element). The resulting binary image (figure 2d) corresponds to the regions of the sample at the k-th depths interval, i.e. the well-focussed regions in figure 2a.
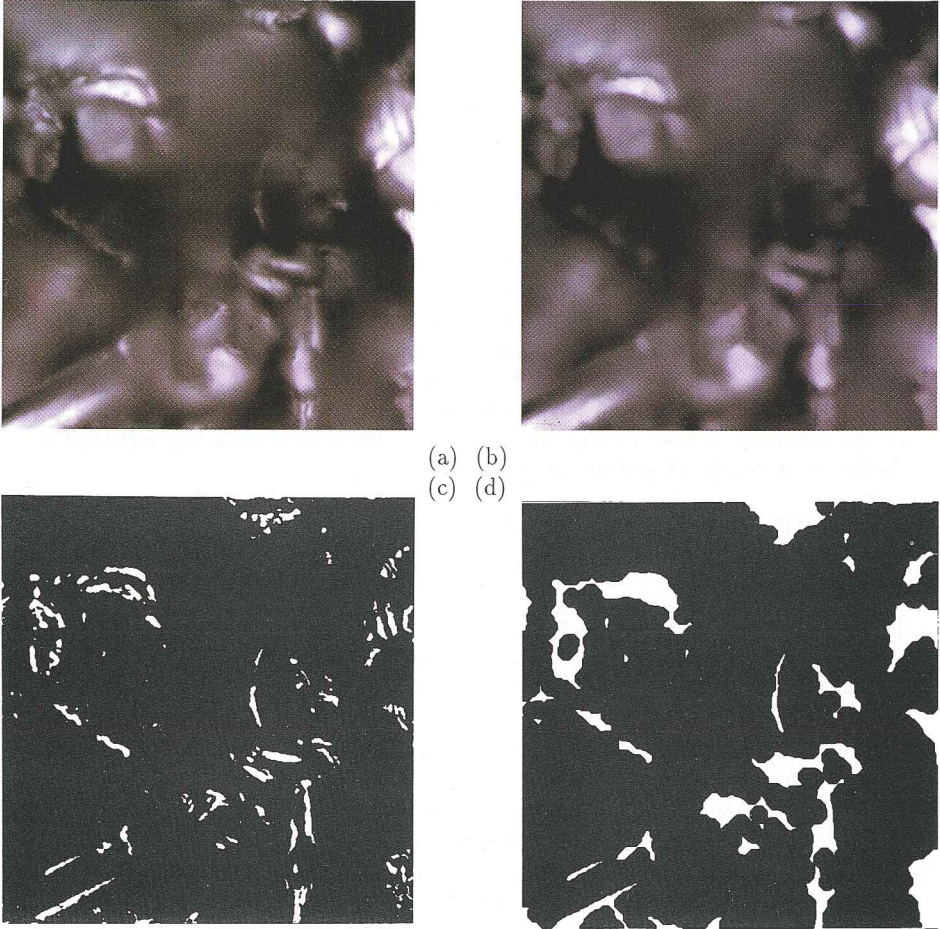

(a) (b)
(c) (d)

Figure 2: Image analysis of a micrograph of a $Cu_{50}Au_{25}Pd_{25}$ powder sample. (a) original optical micrograph, (b) after opening (5 cycles, octagon structuring element), (c) difference of (b) and (a), (d) closing (10 cycles, octagon structuring element) of (c).

This procedure is carried out for each micrograph, $k = 1, \ldots, n$. Finally, the binary images, D_j, of the j-th depth intervals, $j = 1, \ldots, k$, are superimposed by means of logical

OR operations according to

$$E_k = D_1 \cup D_2 \cup \ldots \cup D_k. \qquad (10)$$

The image E_k represents all regions of the material situated at $0 < t < t_k$.
For non-porous materials and non-overlapping surfaces, E_k corresponds to the planar
section at $t = t_k$. The geometrical properties of $E_k, k = 1, \ldots, n$, and its dependence on
the depth t_k characterize the surface morphology of the material. They are analyzed in
terms of the covariance

$$C_k(r) = P(\vec{r}_1 \in E_k, \vec{r}_2 \in E_k), \qquad r = |\vec{r}_1 - \vec{r}_2|. \qquad (11)$$

The covariance is measured by shifting the image E_k by vector $\vec{r}$, calculating the inter-
section of the original and shifted image, and then dividing it by the area of the eroded
frame of the image. For each image, $C_k(r)$ is averaged over two independent perpendicular
shifting directions.

RESULTS

We analyzed a powder sample of the alloy $Cu_{50}Au_{25}Pd_{25}$. A solid casting of the
$Cu_{50}Au_{25}Pd_{25}$ alloy was homogenized then ground with a diamond grinder to form pow-
der. The grinding disk was composed of $70 \pm 10\mu m$-diam particles of diamond embedded
in a 22mm-diam flexible metal disk. Powder produced by this grinding was screened
through a sieve 325 mesh to the inch (2.54cm) with $45\mu m$ openings. Particles larger than
$45\mu m$ were removed from the sample which then contained all particles $< 45\mu m$-diam
produced by grinding. The high ductility of the alloy influences the shape of the particles
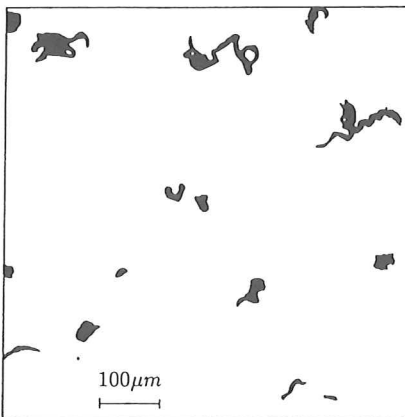produced by grinding. Figure 3 shows the planar projection of a dilute system of particles.

Figure 3: Planar projection of
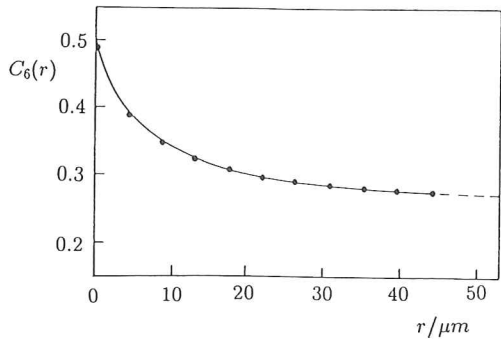$Cu_{50}Au_{25}Pd_{25}$ particles.

Figure 4: Covariance of the image
E_6 of the $Cu_{50}Au_{25}Pd_{25}$ powder sample
obtained at depth $t_6 = 30\mu m$.

Now we study the lateral covariance defined by equation (11) for each depth interval,
$t_k = k\Delta t, k = 1, \ldots, 20, \Delta t = 5\mu m$, with the procedure explained in the previous section.

For each k, 10 different images are analyzed. The quantities $\lambda(t), \bar{V}(t)$ are supposed to vary weakly within a given depth interval k. Inserting $\lambda_k = \lambda(t_k), \bar{V}_k = \bar{V}(t_k)$ the expressions (1 to 9) for homogeneous Boolean models can be used for the interpretation of experimental data. Figure 4 shows the covariance for $t = 30\mu m$. The monotonic decrease can be well reproduced by models of Boolean type. The value $C_k(0) = c_k$ represents the area fraction, and for $r \to r_c$ (r_c is the maximum correlation length) the covariance is to approach c_k^2. This asymptotic value is not reached in the measuring interval $0 \leq r \leq 45\mu m$. Extrapolating $C_k(r)$ to large r-values by means of a straight line having the same ascent as $C_k(r)$ at $r = 45\mu m$, the value c_k^2 is reached at about $100\mu m$. If the maximum correlation length of the investigated structure was of interest the measuring interval should be extended at least to this value.

We consider the variation of the qualitative behaviour of $C_k(r)$ with increasing t_k and check the hypothesis that the bulk structure of the present powder sample can be approximated by a homogeneous Boolean model whereas the surface morphology can be simulated by thinning the bulk model towards the surface. If the hypothesis was true then $C_k(r), 0 \leq t_k \leq t_T$ should behave as the covariance of a Boolean model the volume fraction of which is given by the measured area fraction c_k. (Remember that parameter t_T marks the depth value where the transition from bulk structure to surface region occurs.) At $t = t_T$ the image E_k corresponds to a planar section of the bulk structure if overlapping within the surface region, $0 \leq t \leq t_T$, can be neglected. The latter assumption is justified for powder samples if t_T does not exceed $\bar{l}$ essentially. For $t_k > t_T$ the image D_k is due to the intersection of the layer $(t_k - \Delta t, t_k)$ with the boundary of the pores which are already intersected by the plane $t = t_T$, regions covered by overlapping material deducted. Those pores which are intersected by the layer $(t_k - \Delta t, t_k)$ but not by the plane $t = t_T$ are not visible. Since the pore size is of the order of magnitude of $\bar{l}$, for $t_k \gg t_T + \bar{l}$ each point of the considered sample is covered by one of the images $D_1, D_2, \ldots, D_k$. Consequently, $c_k = 1$ for $t_k \gg t_T + \bar{l}$.

Equations (6, 11) are written in the form

$$\ln\ln\zeta_k = \ln\frac{\lambda_k}{\lambda_b} + \ln[\lambda_b\bar{\gamma}(r)], \quad \zeta_k = \frac{C_k(r) + 1 - 2c_k}{(1 - c_k)^2} \qquad (12)$$

and plotted in figure 5.

Clearly, the $\ln\ln\zeta_k$ curves have the same shape for $k = 1, \ldots, 6$ whereas a qualitative change starts at $k = 7$ and increases with growing k-values. This means that there is a distinct surface morphology within the depth interval $0 \leq t \leq 30\mu m$, and the bulk structure is realized at $t \geq 30\mu m$. The r-dependence of $\ln\ln\zeta_k$ is qualitatively the same for $0 \leq t \leq 30\mu m$. Therefore, the function $\gamma_p(r)$ is also of the same type throughout the surface region. The shifting of the $\ln\ln\zeta_k$ curves for subsequent t_k is due to the decrease of λ_k for $t \to 0$ which corresponds qualitatively to the proposed thinning behaviour. Thus, figure 6 supports the hypothesis that the surface morphology of the present sample can be simulated by a thinning procedure of the bulk model.

We now investigate special aspects of the covariance and its variation with depth t. Figure 6 shows the area fraction $c_k = C_k(0)$ versus t_k. For $t_k \gg t_T + \bar{l}$, the area fraction c_k should tend to 1. This can be attained by a suitable choice of the grey value level in the image processing routine. However, the grey values which optimize the behaviour $c_k \to 1$ for $t_k \gg t_T + \bar{l}$ make worse the resolution of $C_k(r)$ with respect to r. Therefore, we decided to choose a grey value level resulting in $c_k \sim 0.9$ for $t_k \gg t_T + \bar{l}$. That means the image processing routine records about 90% of the complete image D_k. Under the

present experimental conditions, the resulting systematic error is of the same order of magnitude as the statistical one for $0 < t_k \leq 40\mu m$ whereas it dominates for $t_k \geq 40\mu m$ (see figure 6). The experimental data are corrected by the condition

$$\frac{C(r) - c^2}{c(1 - c)} = \frac{C_u(r) - c_u^2}{c_u(1 - c_u)}, \qquad c = \frac{c_u}{c_u^*} \tag{13}$$

where $C(r), c$ are used for the corrected quantities $C_k(r), c_k$, and index u marks the uncorrected data. The asymptotic uncorrected value of the area fraction, c_u^*, is obtained for $t_k >> t_T + \bar{l}$. The special form of expression (13) is used since it is exact without any supposition in the limiting cases $r \to 0$ and $r \to \infty$. In the following, the corrected data are used for quantitative analyses.
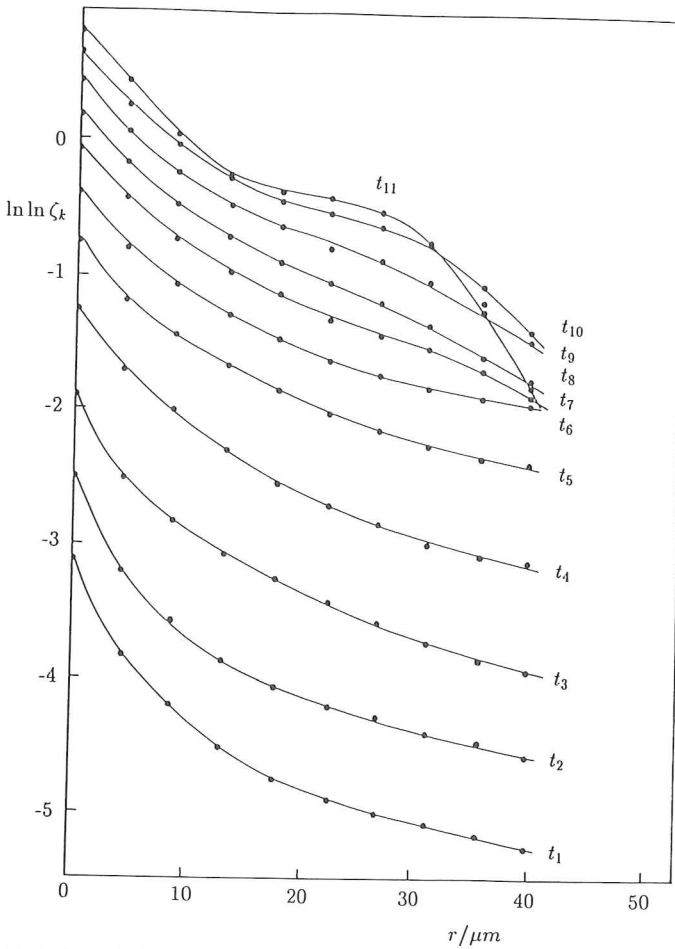

Figure 5: Variation of the covariance (see equation (12)) with profile depth, $t_k = k \cdot 5\mu m$.

The area fraction, c, versus t is given in figure 6 by the solid line. At $t = t_T$ the measured area fraction should approach the packing fraction c_b of the bulk material.

Since the latter was estimated by mass and density measurements to be 0.5 ± 0.1, one obtains for the present sample $t_T = (30 \pm 5)\mu m$ from figure 6. This is in accordance with the value obtained from the qualitative inspection of figure 5. The dependence of the measured area fraction on t for $t > t_T$ should be characteristic of the Boolean model simulating the bulk structure of the sample.

The area fraction, c_k, is related to the linear contact distribution function (equation (5)). For a random point P situated in a pore at $t = t_T$, a point Q can be defined as the intersection of a line $\overline{PQ}$ with the boundary of the pore where $\overline{PQ}$ is perpendicular to the plane $t = 0$, and $t_Q > t_T$. The probability, $H_1(l)$, that the length of the line $\overline{PQ}$ is less than or equal to l is obtained by integrating the density of the linear contact distribution function (5):

$$H_1(l) = 1 - \exp(-l/\bar{l}_B) \tag{14}$$

where $\bar{l}_B$ is the mean chord length of the pores. Assuming the Boolean model to apply the measured area fraction, $c(t)$, should comply with

$$c(t) = c_b + (1 - c_b)H_1(t) \tag{15}$$

for $t < t_T$. In figure 7 the measured area fraction is plotted in the representation $\ln\left[1 - c(t)\right]/[1 - c_b]$ versus t. For $t \geq 30\mu m$ the experimental values follow a linear law according to the linear contact distribution function of the Boolean model. Parameter $\bar{l} = \bar{l}_A$ explained in equations (3, 4, 14) is estimated from the slope of the experimental curve for $t > 30\mu m$. With $c_b = 0.5$ the result is $\bar{l} = 12\mu m$.
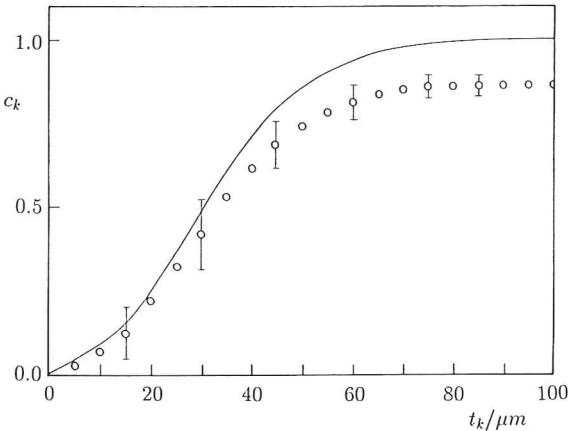

Figure 6: Area fraction, c_k, of the images E_k versus distance, t_k, from reference surface. Uncorrected (o o o) and corrected (solid line) data.The error bars mark the confidence interval for confidence level 0.95.

Now we study the surface morphology of the surface region which we assume to be characterized by thinning the bulk model starting at $t = t_T$ and going to $t = 0$. The variation of $\bar{V}(t_k)$, $k = 1, \ldots, n$, is estimated by means of $\bar{V}(t_k)/\bar{V}(t_T) = [\bar{l}_k/\bar{l}_b]^3$. The mean chord length, $\bar{l}_k$, within k-th depth interval is calculated by equations (4, 8, 9, 11) and numerical differentiation of $C_k(r)$ using the formula $C'_k(0) = [-3C_k(t_1) + 4C_k(t_2) - C_k(t_3)]/2\Delta t$. Solving equation (2) for λ and inserting $\bar{V}(t_k)$ and $c_k = C_k(0)$ the dependence of λ on the depth t can be discussed. The results are shown in figure 8.

Both the mean volume, $\bar{V}(t_k)$, and the mean number density, $\lambda(t_k)$, of effective grains decrease when going from $t = t_T$ to $t = 0$. The decrease of λ means simply that the number of powder particles extending from the bulk region to a certain depth $0 \leq t \leq t_T$ decreases

for $t \to 0$. Probably, only the tips of elongated particles having mean chord lengths of, e.g., $4.4 \mu m$ and $4.6 \mu m$ within depth regions $k = 1$ and 2, respectively, can reach the upper surface layers. This is one reason for the diminution of $\bar{V}(t)$ for $t \to 0$. At $t = t_T$, the mean chord length estimated by equations (4, 8, 9, 11) approaches $\bar{l} = 9 \mu m$ which agrees sufficiently with the value of 12 μm obtained from the linear contact distribution analysis.
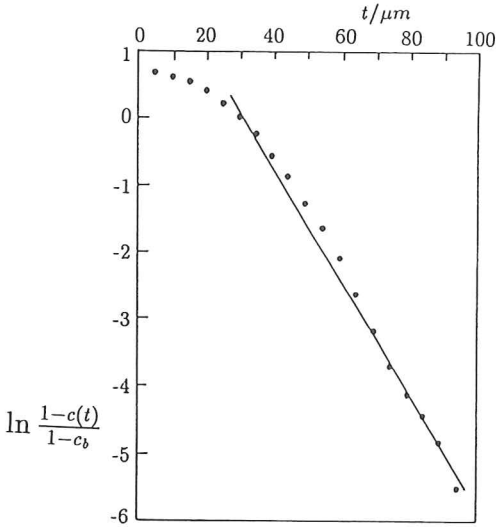

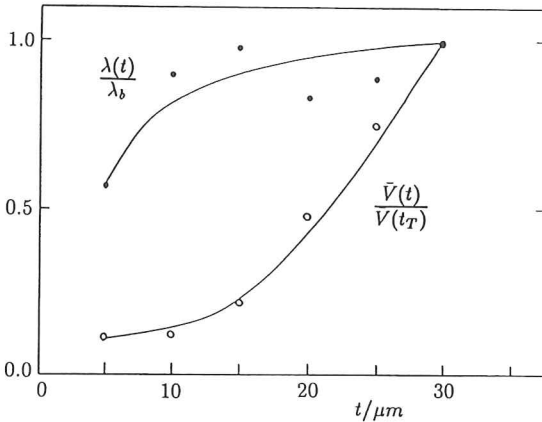Figure 7: Experimental area fraction in the representation $\ln[1 - c(t)]/[1 - c_b]$ versus t.

Figure 8: Estimation of normalized number density, $\lambda(t)/\lambda_b$, and mean volume, $\bar{V}(t)/\bar{V}(t_T)$, of model grains versus t.

DISCUSSION

The method of variable focussing planes has been proven to be a useful tool for the investigation of porous materials and their surface morphology if the method is completed by a careful image analysis. It is also necessary to have available a suitable and variable structure model.

Both bulk structure and surface morphology of the investigated $Cu_{50}Au_{25}Pd_{25}$ powder sample are well described by an inhomogeneous Boolean model. Starting at a reference plane which is parallel to the surface and situated at the top of it, the number density and mean volume of model grains increase with distance from the reference plane. At a certain depth value, number density and size of model grains approach the constant bulk values.

The proposed experimental method is capable both to check qualitative properties of the model and to estimate parameter values for the considered sample.

Future work will be done regarding a more comprehensive statistical analysis and comparison of real structure and model. For example, the spherical contact distribution will be incorporated into the data processing routines. Furthermore, it is of interest to find out morphological parameters which can be estimated by means of the serial focussing method without the Boolean model arguments.

ACKNOWLEDGEMENTS

REFERENCES

Brodsky AM, Urbakh MI. Optical properties of microrough surfaces. Progr Surf Sci 1990; 33: 91-169.

Coster M. Morphological tools for non-planar surfaces analysis. Acta Stereol 1992; 11/Suppl I: 639-650.

Hermann H, Ermrich M. Microabsorption of X-ray intensity in randomly packed powder specimens. Acta Cryst 1987; A43: 401-405.

Jähne B. Digitale Bildverarbeitung, 2. Auflage. Berlin: Springer-Verlag, 1991; p 180.

Savage DE, Kleiner J, Schimke N, Phang YH, Jankowski T, Jacobs J, Kariotis R, Legally MG. Determination of roughness correlations in multilayer films for X-ray mirrors. J Appl Phys 1991; 69: 1411-1424.

Seri-Levi A, Avnir D. Fractal analysis of surface geometry effects on catalytic reactions. Surf Sci 1991; 248: 258-270.

Serra JP. Image analysis and mathematical morphology. London: Academic Press; 1982.

Sparks CJ, Kumar R, Specht ED, Zschack P, Ice GE 1991. Effect of powder sample granularity on fluorescent intensity and on thermal parameters in X-ray diffraction Rietveld analysis. Advances in X-ray Analysis. Plenum publ. Corp., NY vol. 35. p 57.

Stoyan D, Kendall WS, Mecke J. Stochastic geometry and its applications. Chichester: Wiley & Sons; 1987.

Vedel-Jensen EB, Kiêu K. A note on recent results in second-order stereology. Acta Stereol 1991; 11/Suppl I: 569-579.